Acta Crystallographica Section A
Foundations of Crystallography
ISSN 0108-7673

Received 10 November 2005
Accepted 7 June 2006

Fitting valence charge densities at a crystal surface

Laurence D. Marks,[a]* James Ciston,[a] Bin Deng[a] and Arun Subramanian[b]‡

[a]Department of Materials Science and Engineering, Northwestern University, Evanston, IL 60208, USA, and [b]Intel Corporation, Santa Clara, CA 95054, USA. Correspondence e-mail: l-marks@northwestern.edu

A procedure is reported for obtaining a much better initial parameterization of the charge density than that possible from a neutral atom model. This procedure involves the parameterization of a bulk charge density model in terms of simple variables such as bond lengths, which can then be transferred to the problem of interest, for instance a surface. Parameterization is accomplished through the fitting of density functional theory calculations for a variety of crystal distortions. The details of the parameterization are discussed for the specific case of silicon. This parameterized model can then be applied to surfaces or to other problems where an initial higher-order model is needed without the addition of any extra fitted parameters. The non-convexity of the charge density problem is also discussed.

1. Introduction

The most common method to investigate structures is X-ray diffraction, where the scattering of the X-rays depends on the local charge density. Most of the scattering is from the relatively high density region around the atomic cores, and this core region is only very weakly perturbed by the bonding; in most cases, one can use the tabulated scattering factors determined for neutral atoms and get accurate atomic positions. Although the changes in the charge density in a solid with bonding relative to isolated atoms are small – of the order of 1% for the lower-angle structure factors – they can be measured with care. As a specific example, in normal silicon the structure factor for the forbidden 222 reflection is 0.18 e^- (DeMarco & Weiss, 1965) (after subtracting the contribution from thermal vibrations), almost entirely due to the covalent bonding, whereas the structure factor for the 000 reflection is 14 e^-. There is now a fairly large body of literature with experimental charge density measurements [see Coppens (1997), Koritsanszky & Coppens (2001) and Coppens & Iversen (2004) for a recent overview] from X-ray diffraction and bulk crystals.

In contrast to X-rays, swift electrons with the energies typically used in a transmission electron microscope (*i.e.* 100–400 keV) are scattered by the electrostatic potential, related to the charge density (of both the electrons and the positive core) by Poisson's equation. Relatively small changes in the configuration of the valence electrons lead to quite large changes in the shielding of the positive core potential, thereby leading to rather large changes in the intensities, in some cases changes of 50–100% at low scattering angles. Since it is possible to measure with absolute accuracies of 0.1% with sufficient care, one can fit with some appropriate model and from this extract local (*i.e.* atom-by-atom within the unit cell) charge density variations. This has been done in the past with bulk crystals using convergent-electron-beam diffraction (*e.g.* Zuo *et al.*, 1988; Gjonnes & Boe, 1994; Saunders *et al.*, 1995, 1996; Midgley & Saunders, 1996; Holmestad & Birkeland, 1998; Nuchter *et al.*, 1998; Saunders *et al.*, 1999; Zuo *et al.*, 1999; Holmestad *et al.*, 1999; Tsuda *et al.*, 2002; Jiang *et al.*, 2002, 2003), and *via* powder electron diffraction (Avilov *et al.*, 2001; Avilov & Tsirelson, 2001; Tsirelson *et al.*, 2001; Avilov, 2003).

We have very recently managed to perform the same type of analysis at a surface, initially for the MgO (111) $\sqrt{3}\times\sqrt{3}$ R30 surface (Subramanian *et al.*, 2004) and more recently for the Si (001) 2×1H surface (Ciston *et al.*, 2006). To achieve this, we needed to use a procedure slightly different from the normal one, giving the following four-step process.

(*a*) An initial analysis using direct methods and conventional neutral atom structure factors to find the initial model. The direct methods approach for surfaces has been described elsewhere (Marks *et al.*, 1998; Marks, 1999; Marks *et al.*, 2001; Subramanian & Marks, 2004) and will not be discussed further here.

(*b*) A parameterization of the bulk charge density for the material in a form that can be transferred to a refinement of the surface. For MgO, this was a relatively simple spherical model (Subramanian *et al.*, 2004); for silicon, a more complicated approach was needed using bulk bond-centered pseudoatoms (BCPAs), which is the main focus of this paper.

(*c*) Refinement of the structure using these pre-parameterized BCPAs.

(*d*) A final refinement where part of the charge density is allowed to vary and we look for differences relative to the bulk BCPAs. This can be done by a multipole expansion, or some other approach.

‡ Formerly at Department of Materials Science and Engineering, Northwestern University, Evanston, IL 60208, USA.

While other methods might work, the above is the only one we have found to be stable in practice. To understand why, it is important to recognize that most surfaces have relatively large spacings so (particularly with transmission electron diffraction) the effects of charge density variations can be very large, up to 50% of the intensity of relatively strong diffracted beams. As a consequence, a neutral atom refinement can be rather unstable. Using BCPAs fitted to the bulk accounts for about 50–75% of the difference in the charge densities at the surface, so is much more stable. Note that we are not concerned here with whether the final residuals from a fit are better, but rather the more fundamental problem of obtaining a stable reasonably well conditioned fit; our experience with experimental data to date is that the neutral atom starting point is often quite poorly conditioned and may not converge to a reasonable result.

To fit the bulk charge density in a way that can be transferred to a surface is not as simple as one might think. Because of the translational repeat of a bulk material, many different basis sets will give an identical bulk charge density. Depending upon how the charge density is partitioned among the atoms, the basis sets will give completely different results at a surface, in some cases much worse than using neutral atoms. This is particularly true for electron scattering factors which are very sensitive to the long-range behavior of the charge density associated with a particular atom.

The intention of this note is to detail a method of overcoming these issues to obtain a viable parameterization by fitting not simply the bulk material but also a large set of more complicated structures using theoretical charge densities calculated by density functional theory (DFT) methods to ensure a reasonable parameterization that can be extrapolated to fit other structures or a surface. However, before describing the main features of the analysis, it is useful to briefly detail the non-convexity of a charge density fitting since this is crucial to understanding why more than one fit can be used for just the bulk case.

2. Non-convexity of charge density fitting

The key points of a convexity analysis are well described in the optimization literature [for a thorough discussion, see for instance, Rockafellar (1970), Nocedal & Wright (2000) and Bertsekas (2003)], and have been briefly discussed previously in the context of direct methods (Marks *et al.*, 1999). We will briefly perform the same analysis in the context of charge density.

Suppose that we have a charge density $\rho(r)$ which is parameterized in some form

$$\rho(r) \cong \sum_i \rho_a(r - r_i) \tag{1}$$

using some 'atom-like' charge density around each site r_i. We can define as a set all the possible parameterizations that satisfy the condition

$$\left| \rho(r) - \sum_i \rho_a(r - r_i) \right| \leq \text{Tol}, \tag{2}$$

where 'Tol' is some measure of how well we seek to fit the charge density. Let x [$= \sum_i \rho_a(r - r_i)$] represent one parameterization that is a member of the set and y a second. If all the points on the line joining x and y are also members of the set, it is called convex; if some are not, it is non-convex. The key mathematical result is that, if the set for some observable or parameterization is non-convex, in general multiple local solutions exist. (Unfortunately, in some cases only one solution does exist and it is not possible in most cases in any formal mathematical way to determine whether only one or a number of local solutions exist.)

As an example, in terms of a simple multipole-like expansion for a given atom,

$$\rho_a(r) = \rho_{\text{core}}(r) + P_v \kappa^3 \rho_{\text{valence}}(\kappa r) + \sum_{lm} R_l(r) Y_{lm}(\theta, \phi). \tag{3}$$

If we take two different κ values, κ_1 and κ_2, with $\kappa_3 = \lambda\kappa_1 + (1 - \lambda)\kappa_2$, $0 < \lambda < 1$, as representative members of the set of κ values for this atom, since in general

$$\lambda\kappa_1^3 \rho_{\text{valence}}(\kappa_1 r) + (1 - \lambda)\kappa_2^3 \rho_{\text{valence}}(\kappa_2 r) \neq \kappa_3^3 \rho_{\text{valence}}(\kappa_3 r), \tag{4}$$

the densities as a function of position and κ form a non-convex set. (Formally, one should always refer to convexity and non-convexity for the full function of both the positional variables and parameters such as the κ values. We will use here the mathematically 'looser' approach of calling a parameter that leads to a non-convex set a 'non-convex parameter', similarly for a 'convex parameter'.) Any constant multiplier of the spherical harmonics $Y_{lm}(\theta, \phi)$ is a convex parameter, but the radial components [$R(r)$] may not be. For instance, if we write

$$R(r) = \sum_n A_n \exp(-B_n r), \tag{5}$$

the parameters A_n are convex, but B_n are not. (The same analysis holds for an expansion in terms of Slater orbitals.) Furthermore, when one includes expansions about multiple atoms, the angular components of the spherical harmonics also become non-convex. Lastly, the measurements against which the model is being tested, structure factors, are themselves non-convex; the full structure factors (with phases) form a non-convex set. Note that the question of whether the parameters in an expansion or the data are convex or not is completely different from the question of whether the parameters are correlated. Correlated parameters make the problem being solved a little more complicated, but it is still well posed and can be handled by a conventional minimization approach such as least squares, particularly if it includes the second-order part of the Hessian (*e.g.* see Nocedal & Wright, 2000); a non-convex problem is quite different and may require a multisolution approach such as simulated annealing or a genetic algorithm and often has multiple solutions.

This semi-formal analysis demonstrates that there may well be many equally good (or equally bad) expansions that can be used for a bulk material, all of which will give the same overall charge density. This does not mean that they will also give a

Table 1
Dimensions and fractional coordinates of Si in a typical supercell.

Cell parameters	a = 3.7, b = 3.8, c = 12.5 Å, α = 90, β = 90, γ = 90°							
x	0.2500	0.7500	0.2500	0.7500	0.2500	0.7500	0.2500	0.7500
y	0.0000	0.0000	0.5000	0.5000	0.0000	0.0000	0.5000	0.5000
z	0.0620	0.9380	0.1975	0.8025	0.5525	0.4475	0.6875	0.3125

good fit at a surface, or for a more complicated structure. Although there is no formal mathematical proof that we are aware of, it is reasonable that if one can increase the number of parameters against which a fit is performed the overall problem will become 'less non-convex', and the solution more unique. This suggests a parameterization against a database, herein a large set of DFT calculations.

3. Numerical methods

In this paper, we will only describe fits to theoretically calculated valence charge densities. These were generated using the *Wien2k* program (Blaha *et al.*, 2001) [a full-potential all-electron code based on the use of linearized augmented plane-wave + local-orbital (APW+lo) basis sets]. All the calculations for silicon were performed non-spin-polarized with a muffin-tin radius (RMT) of 2.1 Bohr, a maximum angular momentum for the radial wavefunctions ($l_{\max}$) of 10, and a resolution parameter (the smallest RMT*reciprocal-space limit, or RKMAX) of 7 using the generalized gradient approximation (GGA) of Perdew *et al.* (1996).

DFT uses pseudo-orbitals, which do not have to correspond to the true electron wavefunctions but are often taken to be the same. In all cases, the changes in the core densities were very minor (relative to neutral atoms), so the 'valence density' from the DFT results was used as effectively identical to the true valence density. To improve the convergence, only the valence density by itself was calculated and matched.

Refinements were performed using the standard *dnsl* code from the Port Library (Dennis *et al.*, 1981; Gay, 1983; Nocedal & Wright, 2000), which was locally modified to include an additional Broyden–Fletcher–Goldfarb–Shanno (Shanno & Phua, 1974) numerical estimation of the second-order part of the Hessian matrix[1] in the least-squares fit since this was found in practice to be more efficient than the original version.

4. Results

Our approach for silicon was to use a pseudoatom method (Brill, 1959; Phillips, 1968; Brill *et al.*, 1971; Dietrich & Scheringer, 1978; Scheringer & Kutoglu, 1983) since tests indicated that this gave a substantially better fit than a multipolar expansion of the charge density (for silicon, not for all materials) for the same number of adjustable parameters. In the model we used, the total density for each Si atom (at the origin for simplicity) can be written as

$$\begin{aligned}\rho_a(\mathbf{r}) = \rho_{\rm core}(\mathbf{r}) + \rho_{\rm valence}(\mathbf{r}) \\ + C_e\{(\pi/W_+)^{3/2}\exp(-\pi^2|\mathbf{r}-\mathbf{r}_+|^2/W_+) \\ - (\pi/W_-)^{3/2}\exp(-\pi^2|\mathbf{r}-\mathbf{r}_-|^2/W_-)\},\end{aligned} \quad (6)$$

where both the radially symmetric part of the valence density $\rho_{\rm valence}(r)$ as well as the occupancies and the location and shape of the BCPA feature were fitted against the DFT data [see Fig. 1 for a pictorial representation of the third term in equation (6)]. Numerous variants were attempted similar to those described below (*e.g.* one central feature or two, inclusion/exclusion of the negative anti-bonding Gaussian *etc.*), and the final form used a higher-order model (33 parameters plus 1 for the weighting scheme) fitted to 106 theoretical data sets comprising a total of 93142 theoretical structure factors, including both amplitudes and phases. The sets used were calculated from the following variations on a bulk Si lattice:

(i) bulk silicon with a range of lattice parameters from 4.892 to 7.609 Å (32 structures);

(ii) varying the c/a ratio from 1 to 1.3 (0.05 step) while maintaining a constant volume of the unit cell;

(iii) varying the unit-cell volume by scaling the unit-cell axes by 0.925 to 1.15 (0.025 step) for each c/a ratio;

(iv) four supercells (see Table 1 for a typical structure).

The supercells constructed have the structure of distorted bulk Si and are used to capture the averaged longer-range charge density of the valence electrons which cannot be captured with a traditional eight-atom Si unit cell. In addition to these artificial cells, we added to the total data set the experimental values for bulk silicon taken from Saka & Kato (1986) and Cumming & Hart (1988), including a bulk temperature factor as an additional variable for this data set only.

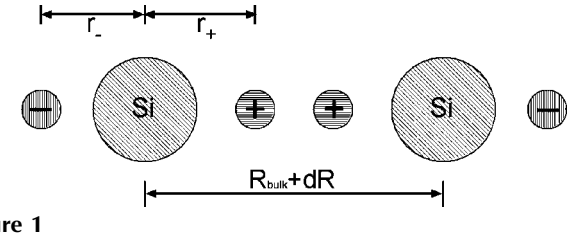

Figure 1
Schematic of bonding model: Si, positive and negatively charged BCPAs as indicated.

[1] In a least-squares fit, the Hessian is defined as $B = J^TJ + \sum_j r_j\nabla^2 r_j$, where J is the Jacobian of the residual (r). Often, only the first term is considered owing to the linearity of the optimization near the solution. However, for systems with large residuals, the second-order part of the Hessian can become significant and it is better to approximate it in some manner to achieve superlinear convergence. For a more complete discussion, see Nocedal & Wright (2000).

Table 2
Slater orbital expansion coefficients for valence levels of Si [notation is that of Su & Coppens (1998)].

3*sp*									
n	2	2	2	2	3	3	3	3	3
c	−0.03405	−0.17788	−0.16001	−0.19069	0.04448	0.26586	1.00000	0.06508	0.23859
ξ	22.0751	4.0132	4.3334	3.2822	15.4242	2.0078	1.3704	1.0085	3.9362

In a tight-binding model, one would expect the magnitude of excess (and depletion) charges to depend exponentially upon the bond distance; this matched the calculated densities rather well. In particular, the charge magnitude of the excess region was parameterized as

$$C_e = \text{occ} \times \exp(-d_1\delta R + d_2\delta R^2 - d_3\delta R^3), \qquad (7)$$

where δR is the fractional change in the Si—Si bond length from the bulk length [$\delta R = \mathrm{d}R/(R_{\text{bulk}} + \mathrm{d}R)$], occ is the fitted occupancy of the central feature, and $d_{1\text{–}3}$ are fitted decay parameters. Because the number of data points used was orders of magnitude greater than the number of fitted parameters, we utilize a non-linear (three-term) exponential for the sake of accuracy without suffering any deleterious effects to goodness-of-fit metrics due to over-fitting. The magnitude of the depletion Gaussian was taken as $-C_e$ to maintain charge neutrality as indicated previously.

The distances of the BCPA features along the axis of each Si—Si pair were fitted independently for both features and parameterized as

$$r_{+,-} = \frac{\text{dac}_{+,-}}{(\delta R - 1)} \exp(\text{dslp}_{+,-}\delta R), \qquad (8)$$

where $\text{dac}_{+,-}$ are fitted distance parameters and $\text{dslp}_{+,-}$ are fitted exponential decay parameters for the positive and negative Gaussians, respectively.

The widths of the Gaussian features were similarly parameterized to the fractional bond-length deviation:

$$W_{+,-} = \sigma_{+,-} + a_{+,-}\delta R + b_{+,-}\delta R^2, \qquad (9)$$

where σ is the first-order width of the Gaussian BCPAs and $a_{+,-}$ and $b_{+,-}$ are fitted parameters for bond-length modification to the width for both the positive and negative BCPAs.

It was determined in a later application of this model to experimental data of the Si(001)-2×1H surface (Ciston *et al.*, 2006) that utilizing only the zero-order term of this expression is sufficient. The bulk Debye–Waller value for silicon (B_{Si}) was also refined in the model using the experimental structure factors for silicon. In this case, we assumed that the BCPA features had the same Gaussian damping as the atoms.

Initial tests were performed using the ground-state silicon Slater-orbital expansion given by Su & Coppens (1998) for the monopole terms (spherically symmetric), with a conventional κ expansion/contraction. Although one can use this with multipole terms to fit simple bulk silicon, we were unable to obtain reasonable fits for the more demanding problem of fitting our large data set. The fact that an isolated atom density from a multiconfigurational SCF calculation (Su & Coppens, 1998) is not a particularly good fit for an atom in a bulk material, particularly for the long-range components, is not surprising, and we believe that this is why the fitting would not work. We found it much superior to use a Slater-orbital wavefunction expansion for the spherically symmetric component, where both the radial exponents and the occupations were allowed to vary as part of the fitting so the long-range components can be adequately matched. Tests indicated that there was no need to incorporate κ-like expansion or contraction of the spherical component as a function of the local environment; it was constant for all the 106 different structures in the data set. Instead, the major non-spherical component of the bond deformation density was fitted by locating excess (positive) charge features modeled by Gaussians along the bond, and a depleted region of negative charge modeled by a negative Gaussian feature opposite the bonds as shown in Fig. 1. The excess and depletion features were constrained to have occupancies of identical magnitude but opposite sign to maintain charge neutrality in the vicinity of each Si atom. Note that the variables we have used are non-convex, so there is the possibility of multiple solutions. However, with the rather large number of data points, we found the solutions to be unique. Note also that, since the charge density from the DFT calculations is everywhere positive, there will be no unphysical negative regions in our parameterization.

Fitted values for the valence level as a '3*sp* shell' with an occupancy of 4 electrons including both the 3*s* and 3*p* in terms of the Slater-orbital expansion coefficients are given in Table 2; the core electrons were taken from the published multi-configurational SCF data (Su & Coppens, 1998) which fit the DFT results for the core pseudo-orbitals very well. (It is not appropriate to separate 3*s* and 3*p* levels in a DFT calculation since they are strongly hybridized and any such separation is prone to error as well as not being physically significant.) It is important to note that, for proper normalization, the wavefunctions computed from the Slater terms in Table 2 must be multiplied by $(2/\pi)^{1/2}$. In all the structures explored, the bond angles were relatively close to the perfect tetrahedral angle. Therefore, the position and occupancy of the Gaussian features along the bond axis were taken to be independent of the bond angle and only a function of the bond length. (If one wanted to parameterize sp^2 *versus* sp^3 bonding terms, a dependence upon bond angles would almost certainly need to be included.)

The Slater orbital expansion terms in Table 2 are somewhat different from a κ expansion (Coppens *et al.*, 1979) of the conventional atomic orbitals (see Fig. 2*a*). From the left side of

Fig. 2(*a*), it is apparent that the Slater orbitals fitted in this work are somewhat expanded compared to those of conventional atomic orbitals. However, a simple κ expansion ($\kappa = 0.96$, chosen for smallest difference) of the atomic orbital does not quite describe what is seen in the full model (Slaters + BCPAs), which has a broader peak and a more quickly decaying tail. Fig. 2(*b*) plots the difference in charge density between the full model and a conventional atomic orbital in the plane of the Si—Si bond.

This model differs from that of a centrally located charge-cloud feature [see Scheringer (1980), Kutoglu *et al.* (1982) and Wu & Spence (2003), for example] in several other ways. The Si-atom cores themselves remain neutral as the positive features between each atomic pair are balanced by negative anti-bond features of the same magnitude. Additionally, the positive Gaussian charges are not centrally located, but form a slightly closer association with each individual atom. The largest and most important difference is in the manner in which this model is eventually applied to experimental data. The purpose of fitting the size, charge and position of the Gaussian features using tens of thousands of theoretical structure factors is to determine numerical constants in closed forms as functions of the Si—Si bond length which describes these properties. Upon fitting an actual experimental data set, these functions are used as an initial second-order model to describe to quite a high degree of accuracy the bonding features (of Si—Si pairs only) at a surface with no adjustable parameters, because the excess charge in the model is a function *only* of the bond length. In addition, the Slater-orbital expansion terms are taken to be those refined from this theoretical analysis and remain fixed when fitting experimental data. The atomic positions and temperature factors are fitted in the typical manner as if the atoms were neutral, and the bonding information is incorporated into each iteration of the fit by utilizing this parameterization. In the experimental fit, the BCPAs are taken to have the same temperature factors as the Si they are bound to. A more complete third-order model with, for instance, additional multipolar terms would then incorporate perturbations about this second-order model to describe the charge density changes at a surface. Since the second-order model will be much closer to the true density than a zero-order neutral atom model, the perturbations needed for a complete description will be smaller so the whole problem becomes much better conditioned.

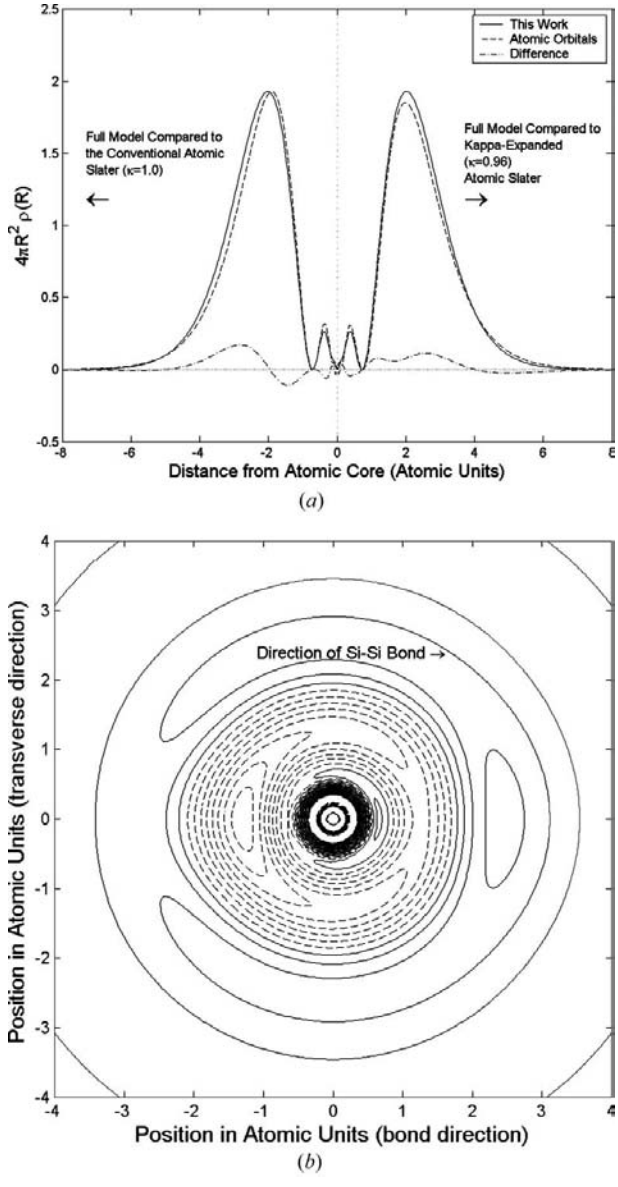

Figure 2
(*a*) Fitted Slater orbitals of the full model compared toh both conventional and κ-expanded atomic Slater expansion. (*b*) Charge density difference between the full model and atomic model in the plane of an Si—Si bond (dashed lines negative, contour interval 0.01 e Å^{-3})

A subtle question concerns how one should treat the intensities as a function of scattering angle. To obtain a representative fit of the long-range components (small scattering vector), which are the ones most significant for a charge density analysis (particularly for electron diffraction or for a surface), it is reasonable to weight these more heavily, for instance by using a Debye–Waller-like scheme with

$$\text{weight} = \exp(-As^2), \tag{10}$$

where s is the length of the scattering vector and A is adjustable. A weighting approach similar to this is also appropriate because of the numerical errors in any DFT calculation. All DFT calculations (and also other *ab initio* methods) use a limited range of sampling in reciprocal space (in a rather complicated fashion that we will not expand upon here); there are also numerical errors due to how the charge density is represented near the atomic nuclei, truncation effects or kinks at the edge of the muffin tins, and the fact that the density functionals used are themselves only approximately correct. As a consequence, the larger s values are less reliable. A reasonable value for the weighting term A in equation (10) is going to be something similar to what one will have in any experimental data from thermal vibrations; we do not believe that there is any 'correct' value. In practice, we have not found that this term has a major effect, and used a value of $A = 1$.

Table 3
Numerical coefficients of the second-order model.

occ	0.15489
d_1	0.48608
d_2	−0.58791
d_3	6.8459
dac_-	1.4995
dac_+	−1.6672
dslp_-	−0.05696
dslp_+	0.04837
σ_-	9.6274
σ_+	13.5763
a_-	1.2121
a_+	−3.5310
b_-	−4.6612
b_+	0 (not refined)
B_{Si}	0.4657

All of the numerical coefficients included in this section correspond to a bonding model in which there are two features of charge excess between each Si pair. The values of these coefficients are given in Table 3 and represent the model we found to yield the best results when fitting actual surface diffraction data. Analysis of similar models (*e.g.* single-bond feature, features of far different sizes *etc.*) was performed which yield entirely different values for these coefficients, but the resulting models fit nearly as well to the data emphasizing the overall non-convexity of the problem.

The numerical uncertainties in these parameters do not arise from the residuals of the fitting itself but are instead dominated by the inherent errors of the DFT calculations which were used to generate the 93142 data points for refinement. DFT uses pseudo-orbitals which do not have to correspond to the true electron wavefunctions but are often taken to be the same. An example of one manifestation of these errors is that the APW+lo method used herein produces a discontinuity in the first derivative of the charge density at the edge of the muffin tin. For a more complete characterization of the errors in the DFT charge density of silicon, see Zuo *et al.* (1997) who estimates a χ^2 of over 4 for GGA methods. In light of these considerations, the error of the values in Table 3 should be taken to be on the order of 1%. As an alternative gauge of the accuracy of the model, Table 4 shows the calculated values for the bulk silicon structure factors obtained from our model compared to both the experimental data and our calculated GGA results.

From the GOF values in Table 4, it is clear that our second-order model is a significantly better fit to the experimental data than the GGA structure factors even thought we fitted the model to the valence charge density calculated by GGA. The difference, therefore, must be due to discrepancies in the core-electron wavefunctions since the second-order model utilized a Slater orbital expansion for the core levels rather than fitting to the GGA results. It is known that GGA does not perform as well with core electrons compared to valence electrons due to self-interactions. We did not use any core self-interaction corrections (such as given by Friis *et al.*, 2003) to the GGA calculations because although these corrections improve the core-electron density they yield poor energies for the core states.

Table 4
Comparison of experimental and theoretical Si form factors in units of electrons per atom.

Experimental errors are given in parentheses. A goodness-of-fit factor (GOF) was also computed for both sets of calculated form factors. The GGA result was fitted with a Debye–Waller (B) factor of 0.4662 Å^2.

hkl	Experiment†	APW+lo, GGA‡	Second-order model
111[b]	10.6025 (29)	10.6025	10.6009
220[b]	8.3881 (22)	8.3897	8.3910
311[b]	7.6814 (19)	7.6882	7.6820
222[b]	0.182 (1)	0.1654	0.1816
400[b]	6.9958 (12)	6.9999	6.9955
331[b]	6.7264 (20)	6.7135	6.7264
422[b]	6.1123 (22)	6.1020	6.1096
333[b]	5.7806 (21)	5.7680	5.7729
511[b]	5.7906 (27)	5.7884	5.7921
440[b]	5.3324 (20)	5.3263	5.3385
531[a]	5.0655 (17)	5.0611	5.0739
620[a]	4.6707 (9)	4.6668	4.6738
533[a]	4.4552 (11)	4.4538	4.4545
444[b]	4.1239 (18)	4.1168	4.1186
711[a]	3.9282 (22)	3.9312	3.9354
551[b]	3.9349 (34)	3.9328	3.9352
642[b]	3.6558 (54)	3.6495	3.6507
731[a]	3.4919 (11)	3.4928	3.4934
553[a]	3.5055 (14)	3.4944	3.4936
800[b]	3.2485 (34)	3.2526	3.2528
733[a]	3.127 (14)	3.1208	3.1194
822[a]	2.9111 (15)	2.9148	2.9133
660[b]	2.9143 (16)	2.9150	2.9133
555[b]	2.8009 (21)	2.7988	2.7991
751[a]	2.8006 (25)	2.8017	2.7991
840[a]	2.6200 (7)	2.6254	2.6227
911[a]	2.5325 (8)	2.5275	2.5245
753[a]	2.5274 (29)	2.5261	2.5246
664[a]	2.3677 (9)	2.3762	2.3726
844[b]	2.1506 (24)	2.1605	2.1562
GOF§	N/A	25.1	11.4

† Data taken from (*a*) Saka & Kato (1986) and (*b*) Cumming & Hart (1988). ‡ APW+lo: calculations using the GGA of Perdew *et al.* (1996). § $\mathrm{GOF} = 1/N \sum_i (1/\sigma_i^2)(f_i^{\mathrm{theory}} - f_i^{\mathrm{exp}})^2$.

5. Discussion

The strategy that we have used herein, fitting a larger data set from DFT results, is one that we believe is generally applicable and will give much more stable results than just starting from neutral (unbonded) atoms. It is an extension of previous work on an MgO surface (Subramanian *et al.*, 2004) where a spherical (first-order) deformation model was adequate for the initial refinements yielding a χ^2 of 1.5, whereas the neutral atom (zero-order) fit refined to a χ^2 of approximately 3, emphasizing the necessity of accounting for the effects of bonding. Using the second-order silicon parameterization described herein, we have been able successfully to refine the charge density of an H-atom-terminated Si (001) 2×1 surface (Ciston *et al.*, 2006) including stably refining the H-atom positions; the H atoms were unstable in a neutral atom refinement and would refine to a (B) temperature factor of >100 or to chemically unrealistic locations (Si—H bond distances of 5 Å or more). This is why a previous analysis (Lauridsen *et al.*, 2000) using a neutral atom approach for the same data was unable to find the H-atom positions. With the second-order model alone (*i.e.* no additional charge defor-

mation), the H-atom positions refined stably giving an Si—H bond distance of 1.51 Å and an integrated bond density between two of the surface Si atoms of 0.31 electrons, which compared well with the results of DFT calculations (at 0 K) of 1.49 Å (Ciston *et al.*, 2006) and 0.37 electrons.

The BCPA approach is of course not the only one, and in some cases a multipolar expansion of a large data set might give better results, where 'better' should be taken in a semi-formal mathematical sense to indicate an equal level of accuracy with a smaller number of adjustable parameters. One thing that we feel should be stressed is the importance in all cases of using a reasonable basis set to fit the radially symmetric part of the density, not just a simple κ fit with one adjustable parameter, particularly for applications using electron diffraction data. Conventional neutral atom expansions are based upon Hartree–Fock or multiconfigurational Hartree–Fock analyses with Slater or Gaussian orbitals. While these will almost certainly be quite good near the core, they are very likely to be somewhat inaccurate for the long-range components. Since these have a large effect on the scattering factors at small s values, where electron diffraction is most sensitive, just allowing for a simple expansion/contraction is not in general adequate.

This work was supported by the MRSEC program of the National Science Foundation (DMR-0076097) at the Materials Research Center of Northwestern University (BD) and the National Science Foundation (DMR-0455371).

References

Avilov, A., Lepeshov, G., Pietsch, U. & Tsirelson, V. (2001). *J. Phys. Chem. Solids*, **62**, 2135–2142.

Avilov, A. S. (2003). *Z. Kristallogr.* **218**, 247–258.

Avilov, A. S. & Tsirelson, V. G. (2001). *Crystallogr. Rep.* **46**, 556–571.

Bertsekas, D. P. (2003). *Convex Analysis and Optimization*, 1st ed. New York: Athena Scientific.

Blaha, P., Schwarz, K., Madsen, G. K. H., Kvasnicka, D. & Luitz, J. (2001). *An Augmented Plane Wave + Local Orbitals Program for Calculating Crystal Properties.* Technische Universität Wien, Austria.

Brill, R. (1959). *Z. Elektrochem.* **63**, 1088–1091.

Brill, R., Dietrich, H. & Dierks, H. (1971). *Acta Cryst.* B**27**, 2003–2018.

Ciston, J., Marks, L. D., Feidenhans'l, R., Bunk, O., Falkenberg, G. & Lauridsen, E. M. (2006). Submitted.

Coppens, P. (1997). *X-ray Charge Densities and Chemical Bonding*, 1st ed. Oxford University Press.

Coppens, P., Guru Row, T. N., Leung, P., Stevens, E. D., Becker, P. J. & Wang, Y. W. (1979). *Acta Cryst.* A**35**, 63–72.

Coppens, P. & Iversen, B. (2004). *Coord. Chem. Rev.* **249**, 179–195.

Cumming, S. & Hart, M. (1988). *Aust. J. Phys.* **41**, 423.

DeMarco, J. J. & Weiss, R. J. (1965). *Phys. Rev.* **137**, 1869–1871.

Dennis, J. E., Gay, D. M. & Welsch, R. E. (1981). *ACM Trans. Math. Softw.* **7**, 348–368.

Dietrich, H. & Scheringer, C. (1978). *Acta Cryst.* B**34**, 54–63.

Friis, A. J., Madsen, G. K. H., Larsen, F. K., Jiang, B., Marthinsen, K. & Holmestad, R. (2003). *J. Chem. Phys.* **119**, 11359–11366.

Gay, D. M. (1983). *ACM Trans. Math. Softw.* **9**, 503–524.

Gjonnes, K. & Boe, N. (1994). *Micron*, **25**, 29–44.

Holmestad, R. & Birkeland, C. R. (1998). *Philos. Mag.* A**77**, 1231–1254.

Holmestad, R., Birkeland, C. R., Marthinsen, K., Hoier, R. & Zu, J. M. (1999). *Microsc. Res. Tech.* **46**, 130–145.

Jiang, B., Zuo, J. M., Chen, Q. & Spence, J. C. H. (2002). *Acta Cryst.* A**58**, 4–11.

Jiang, B., Zuo, J. M., Jiang, N., O'Keeffe, M. & Spence, J. C. H. (2003). *Acta Cryst.* A**59**, 341–350.

Koritsanszky, T. S. & Coppens, P. (2001). *Chem. Rev.* **101**, 1583–1628.

Kutoglu, A., Scheringer, C., Meyer, H. & Schweig, A. (1982). *Acta Cryst.* B**38**, 2626–2632.

Lauridsen, E. M., Baker, J., Nielsen, M. & Feidenhans'l, R. (2000). *Surf. Sci.* **453**, 18–24.

Marks, L. D. (1999). *Phys. Rev. B*, **60**, 2771–2780.

Marks, L. D., Bengu, E., Collazo-Davila, C., Grozea, D., Landree, E., Leslie, C. & Sinkler, W. (1998). *Surf. Rev. Lett.* **5**, 1087–1106.

Marks, L. D., Erdman, N. & Subramanian, A. (2001). *J. Phys. Condens. Matter*, **13**, 10677–10687.

Marks, L. D., Sinkler, W. & Landree, E. (1999). *Acta Cryst.* A**55**, 601–612.

Midgley, P. A. & Saunders, M. (1996). *Contemp. Phys.* **37**, 441–456.

Nocedal, J. & Wright, S. J. (2000). *Numerical Optimization.* New York: Springer.

Nuchter, W., Weickenmeier, A. L. & Mayer, J. (1998). *Phys. Status Solidi A*, **166**, 367–379.

Perdew, J. P., Burke, K. & Ernzerhof, M. (1996). *Phys. Rev. Lett.* **77**, 3865–3868.

Phillips, J. C. (1968). *Phys. Rev.* **166**, 832–838.

Rockafellar, R. T. (1970). *Convex Analysis*, 1st ed. Princeton University Press.

Saka, T. & Kato, N. (1986). *Acta Cryst.* A**42**, 469–478.

Saunders, M., Fox, A. G. & Midgley, P. A. (1999). *Acta Cryst.* A**55**, 471–479.

Saunders, M., Midgley, P., Vincent, R. & Steeds, J. (1996). *J. Electron Microsc.* **45**, 11–18.

Saunders, M., Midgley, P. A. & Vincent, R. (1995). *Bonding Charge Density Measurements in Group IV Elements*, Vol. 147, *Electron Microscopy and Analysis 1995*, pp. 125–128. Bristol: Institute of Physics Publishing Ltd.

Scheringer, C. (1980). *Acta Cryst.* A**36**, 205–210.

Scheringer, C. & Kutoglu, A. (1983). *Acta Cryst.* A**39**, 899–901.

Shanno, D. F. & Phua, K. H. (1974). *ACM Trans. Math. Softw.* **2**, 97–94.

Su, Z. W. & Coppens, P. (1998). *Acta Cryst.* A**54**, 646–652.

Subramanian, A. & Marks, L. D. (2004). *Ultramicroscopy*, **98**, 151–157.

Subramanian, A., Marks, L. D., Warschkow, O. & Ellis, D. E. (2004). *Phys. Rev. Lett.* **92**, 026101-1–4

Tsirelson, V. G., Avilov, A. S., Lepeshov, G. G., Kulygin, A. K., Stahn, J., Pietsch, U. & Spence, J. C. H. (2001). *J. Phys. Chem.* B**105**, 5068–5074.

Tsuda, K., Ogata, Y., Takagi, K., Hashimoto, T. & Tanaka, M. (2002). *Acta Cryst.* A**58**, 514–525.

Wu, J. S. & Spence, J. C. H. (2003). *Acta Cryst.* A**59**, 495–505.

Zuo, J. M., Blaha, P. & Schwarz, K. (1997). *J. Phys. Condens. Matter*, **9**, 7541–7561.

Zuo, J. M., Kim, M., O'Keeffe, M. O. & Spence, J. C. H. (1999). *Nature (London)*, **401**, 49–52.

Zuo, J. M., Spence, J. C. H. & O'Keeffe, M. (1988). *Phys. Rev. Lett.* **61**, 353–356.